Int J Thermophys (2015) 36:967–972
DOI 10.1007/s10765-014-1716-z

CrossMark

Depth Profiling of Electronic Transport Properties in H^+-Implanted n-Type Silicon

Rui Tai · Chinhua Wang · Jingpei Hu · Andreas Mandelis

Received: 3 December 2013 / Accepted: 1 August 2014 / Published online: 24 August 2014
© Springer Science+Business Media New York 2014

Abstract A depth profiling theory for electronic transport properties (carrier diffusivity and lifetime) in ion-implanted semiconductor wafers using infrared photocarrier radiometry (PCR) is proposed. The ion-implanted inhomogeneous sample was sliced into many virtual sub-layers along the depth direction so that the continuously variable electronic properties across the whole thickness can be considered as uniform in each incremental slice. A recursion relationship among the slices was obtained, and the overall PCR signal was built based on contributions from each slice. Experimental lifetime and electronic diffusivity reconstructions of depth profiles at two ion doses (3×10^{14} cm^{-2} and 3×10^{15} cm^{-2}) and several implantation energies (from 0.75 MeV to 2.0 MeV) have been demonstrated.

Keywords Depth profile · Electronic transport properties · Photocarrier radiometry · Reconstruction

1 Introduction

Accurate control and evaluation of the electronic properties of ion-implanted semiconductors have been an important topic in industry. Frequency-domain photocarrier radiometry (PCR), a dynamic modulated photoluminescence technique, was found

R. Tai · C. Wang (✉) · J. Hu
Institute of Modern Optical Technologies & Collaborative Innovation Center of Suzhou Nano Science and Technology, Jiangsu Key Lab of Advanced Optical Manufacturing Technologies & MOE Key Lab of Modern Optical Technologies, Soochow University, Suzhou 215006, China
e-mail: chinhua.wang@suda.edu.cn

A. Mandelis
Center for Advanced Diffusion-Wave Technologies, Department of Mechanical and Industrial Engineering, University of Toronto, Toronto, ON M5S 3G8, Canada

to be a sensitive method for characterization and subsurface defect imaging of semiconductor materials. There have been several theoretical and experimental studies for the PCR response of ion-implanted semiconductors [1–7]. Li et al. [6] and Wang et al. [7] developed three- and two-layer theoretical models, respectively, which explain the PCR signal dependence on the ion implantation dose. Both of those models, however, consider the ion-implanted sample as two or three "effective" layers in which the ion-traversed region, the eventual ion residence region, and the intact substrate are assumed to be "uniform." Although the assumption of "effective layer" models can explain phenomena observed in ion-implanted samples, it is, however, inaccurate and impractical for representing real ion implantation in samples where the electronic properties are continuously varying along the axis perpendicular to the sample surface across the whole implanted thickness. In this work, a theoretical model is proposed to reconstruct the depth profiles of the continuously variable electronic transport properties in the ion-implanted semiconductor wafers. The inhomogeneous wafer is sliced into many virtual sub-layers along the depth direction so that the continuously varied electronic properties across the whole thickness can be considered as uniform in each slice increment. The effectiveness of this model is validated through experimental data from H^+-implanted wafers.

2 Theoretical Model

An ion-implanted inhomogeneous semiconductor can be described using a multilayer model. The geometry of the ion-implanted sample and incident laser beam is shown in Fig. 1. The thickness of each sliced layer is denoted by L_j $(j = 1, 2, \ldots, M)$, in which L_1 is the ion-traversed layer, L_M is the intact substrate, and L_2 to L_{M-1} are the actual inhomogeneous layers. L_e is the depth of the inhomogeneous region between the ion-traversed region and the intact substrate, which can be expressed as $L_\mathrm{e} = \sum_{j=2}^{M-1} L_j$. The exciting laser beam is assumed to be of finite size with a Gaussian profile, $\exp(-r^2/w^2)$, where w is the laser beam spot size.

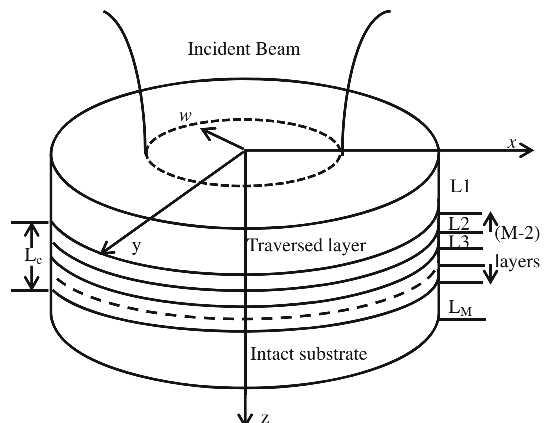

Fig. 1 Configuration of an ion-implanted inhomogeneous semiconductor structure

The optically injected three-dimensional carrier densities $N_j(r, z, \omega)$ for each layer in the model are calculated from the following carrier transport equations:

$$\nabla^2 N_j(r, z, \omega) - \sigma_j^2 N_j(r, z, \omega) = -\frac{G_j(r, z, \omega)}{D_j}, \quad (j = 1, 2, \ldots, M), \tag{1}$$

D_j is the carrier diffusion coefficient. The complex plasma-wave vector σ_j is defined as: $\sigma_\mathrm{j} = \sqrt{(1 + \mathrm{i}\omega\tau_j)/(D_j\tau_j)}$, where τ_j is the carrier lifetime for each layer. G_j is the source part in each layer, which is proportional to $\exp(-\frac{r^2}{w^2} - \alpha_j z)$, with α_j being the absorption coefficient of each layer. The boundary conditions for the carrier density wave at the front and the rear surface are

$$D_1 \frac{\partial N_1(r, z, \omega)}{\partial z} = s_1 N_1(r, z, \omega), \quad z = 0, \tag{2}$$

$$D_M \frac{\partial N_M(r, z, \omega)}{\partial z} = -s_{M+1} N_M(r, z, \omega), \quad z = L_1 + L_2 + \cdots + L_M \tag{3}$$

s_1 and s_{M+1} are the effective recombination velocities at the front and rear surfaces of the wafer, respectively. The boundary conditions for the carrier wave at other interfaces $(j = 2, \ldots, M)$ are

$$N_{j-1}(r, z, \omega) = N_j(r, z, \omega), \quad z = L_1 + L_2 + \cdots + L_{j-1}, \tag{4}$$

$$D_{j-1} \frac{\partial N_{j-1}(r, z, \omega)}{\partial z} = D_j \frac{\partial N_j(r, z, \omega)}{\partial z} - s_j N_j(r, z, \omega), \quad z = L_1 + L_2 + \cdots + L_{j-1}. \tag{5}$$

Here s_j is the effective recombination velocity at each interface, in which only $s_2 \neq 0$ due to the eventual ion residence region at $z = L_1$, and $s_3, s_4, \ldots, s_M = 0$ at all other virtual interfaces. By taking the Hankel transform of the carrier transport equations, Eq. 1 and the boundary conditions, Eqs. 2 to 5, the solutions for the free-carrier densities in Hankel space can be obtained:

$$\tilde{N}_j(\lambda, z, \omega) = \tilde{A}_j \exp(-\beta_j z) + \tilde{B}_j \exp(\beta_j z) + \tilde{E}_j \exp(-\alpha_j z), \quad j = 1, 2, \ldots, M. \tag{6}$$

Here $\beta_j = \sqrt{\sigma_j^2 + \lambda^2}$ and λ is the Hankel variable. Constants $\tilde{E}_j$ denote the Hankel transform of the source. A recursion relation of coefficients $\tilde{A}_j$ and $\tilde{B}_j$ in Eq. 6 for the adjacent layers can be derived from the boundary conditions:

$$\begin{bmatrix} \tilde{\mathrm{A}}_j \\ \tilde{\mathrm{B}}_j \end{bmatrix} = \begin{bmatrix} t_{11}^{j-1} t_{12}^{j-1} \\ t_{21}^{j-1} t_{22}^{j-1} \end{bmatrix} \begin{bmatrix} \tilde{\mathrm{A}}_{j-1} \\ \tilde{\mathrm{B}}_{j-1} \end{bmatrix} + \begin{bmatrix} c_1^{j-1} \\ c_2^{j-1} \end{bmatrix}, \quad j = 1, \ldots, M. \tag{7}$$

The analytical expressions of the coefficients t_{mn}^j and c_m^j $(m, n = 1, 2)$ in the transform matrix depend on D_j, β_j, s_j, L_j, and α_j. By applying the recursion relation in Eq. 7,

the coefficients for each layer can be obtained. The final signal in Hankel space can be expressed as a summation of the signal contributions from all the layers:

$$\tilde{S}_{\mathrm{PCR}}(\omega) = \int_0^{L_1} \tilde{N}_1(\lambda, z, \omega)\mathrm{d}z + \sum_{j=2}^{M} \int_{L_1+\cdots+L_{j-1}}^{L_1+\cdots+L_j} \tilde{N}_j(\lambda, z, \omega)\,\mathrm{d}z. \quad (8)$$

Taking into account the collective efficiency of the detector, the final PCR signal to be detected is thus expressed as

$$S_{\mathrm{PCR}}(\omega) = C(\omega) \int_0^{\infty} \tilde{S}_{\mathrm{PCR}}(\omega)\, J_1(\lambda a)\mathrm{d}\lambda. \quad (9)$$

Here $C(\omega)$ is a proportionality factor including instrumental factor, independent of the electronic transport properties, and a is the radius of the detector's aperture.

3 Experiment and Fitting Results

The experimental setup has been described in detail elsewhere [8]. Eight n-Si wafer samples were divided into two sets which were H^+ implanted with a dose of $3 \times 10^{14}\,\mathrm{cm}^{-2}$ and $3 \times 10^{15}\,\mathrm{cm}^{-2}$, respectively, and each set was implanted at different energies varying from 0.75 MeV to 2.00 MeV. The PCR amplitude and phase behavior were recorded as a function of the modulation frequency with a lock-in amplifier. Frequency scans were performed from 0.5 kHz to 100 kHz with a total of 31 points, logarithmically spaced. Multiparameter fitting of the experimental data to the theoretical model was performed via a least-squares process.

As shown in Fig. 1, electronic transport properties (D_j and τ_j) in inhomogeneous region L_e are expected to change monotonically due to the ion diffusion effect along the depth direction. Two formulas, which are capable of describing arbitrary monotonic and saturated depth profiles for the carrier lifetime (τ) and carrier diffusivity (D) are thus assumed [9]:

$$K = K_0 \left(\frac{1 + \Delta \exp(-qz)}{1 + \Delta} \right)^2, \quad \Delta = \frac{1 - \sqrt{K_\infty / K_0}}{\sqrt{K_\infty / K_0} - \exp(-qL_\mathrm{e})}, \quad K = D, \tau \quad (10)$$

K_0 and K_∞ represent the initial and the saturation value of the carrier diffusivity (D) and carrier lifetime (τ) in the inhomogeneous region, respectively. q represents the gradient of the change for the electronic transport properties.

The amplitude and phase behavior of the PCR signal as a function of frequency and the corresponding best-fitted theoretical curves for two sets of samples with different doses are shown on the left half part of Fig. 2a1, a2, b1, b2. In the fitting process, K_∞, i.e., the saturated value of the carrier life time or carrier diffusivity which is the same as that of the intact substrate is assumed to be known. Other parameters, i.e., q, K_0, and L_e as well as the surface recombination velocities in Eq. 5 are the fitting parameters. Good agreement between the best-fitted lines and the experimental data

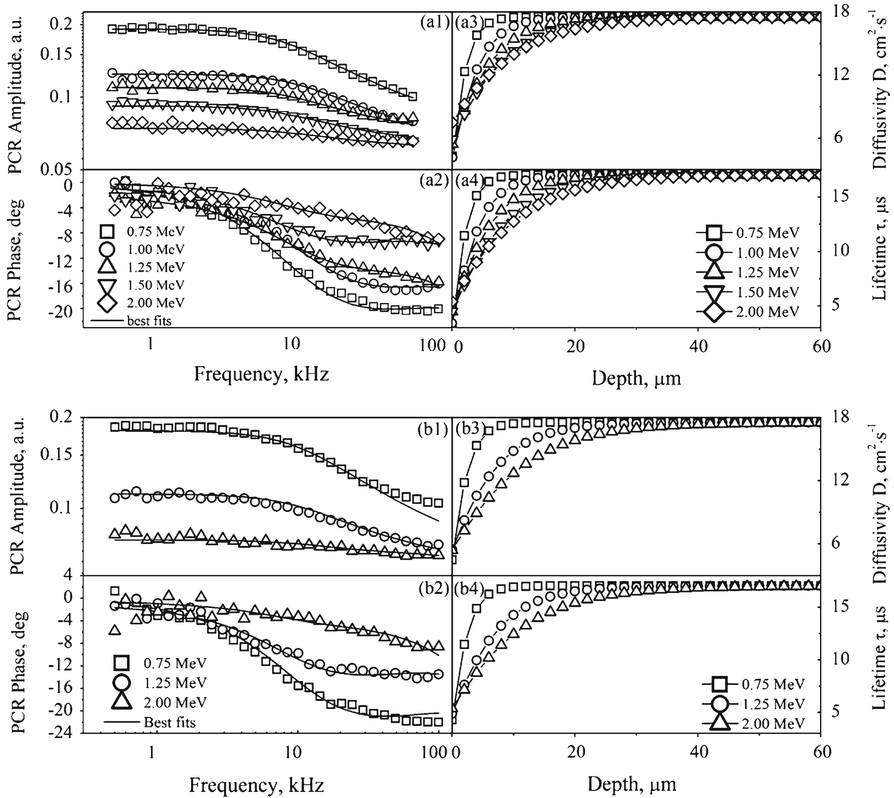

Fig. 2 Experimental frequency dependence of PCR amplitudes (a1, b1) and phases (a2, b2), and the corresponding best-fitted theoretical curves; the reconstructed depth profiles for the carrier diffusivity (a3, b3) and the carrier lifetime (a4, b4) for H^+-implanted semiconductor wafers at several implantation energies with *a* and *b* corresponding to the implantation doses of 3×10^{14} cm^{-2} and 3×10^{15} cm^{-2}, respectively

is obtained. The depth profiles for the carrier diffusivity and the carrier lifetime in the inhomogeneous region between the ion-traversed layer and the intact substrate for all samples are illustrated on the right half of Fig. 2a3, a4, b3, b4. It is seen that for each set of samples with the same implantation dose, the thickness of the inhomogeneous part in the substrate increases with increasing implantation energy, as expected. The corresponding best-fitted results of L_e for the first set of samples (dose of 3×10^{14} cm^{-2}) are 10.5 μm, 20 μm, 30.6 μm, 40.7 μm, and 50.9 μm for implantation energies of 0.75 MeV, 1.0 MeV, 1.25 MeV, 1.5 MeV, and 2.0 MeV, respectively. For the second set of samples (dose of 3×10^{15} cm^{-2}), the best-fitted results of L_e are 11.8 μm, 35.2 μm, and 54.6 μm for implantation energies of 0.75 MeV, 1.25 MeV, and 2.0 MeV, respectively. It should be noted that the effects of different fitted parameters on the PCR signal can be well deconvoluted from each other in the meaningful range of semiconductor physics, which also have been verified in previous papers [6,7].

4 Conclusion

In this work, a new theoretical model has been developed to reconstruct the depth profiles of the electronic properties in H^+-implanted wafers. Compared to the existing two- and three-layer models, an inhomogeneous region beneath the ion residence layer has been assumed making this model more practical and precise. Experimental data are fitted to the multilayer model, and good consistency between the theory and the experiments has been obtained, showing the effectiveness of the theoretical model.

Acknowledgments This work was supported by a Grant from the National Natural Science Foundation of China Contract No. 60877063, Scientific Research Foundation for Returned Scholars, Ministry of Education of China, and the Project of the Priority Academic Program Development (PAPD) of Jiangsu Higher Education Institutions.

References

1. X. Liu, B. Li, Q. Huang, Chin. Phys. B **19**, 097201 (2010)
2. A. Gutiérreza, M.E. Rodríguez-García, J. Giraldo, Physica B **406**, 3687 (2011)
3. L. Qin, J.Y. Liu, Y. Wang, Appl. Mech. Mater. **268–270**, 1623 (2013)
4. J. Batista, A. Mandelis, D. Shaughnessy, Appl. Phys. Lett. **82**, 4077 (2003)
5. A. Mandelis, J. Appl. Phys. **97**, 083508 (2005)
6. B. Li, D. Shaughnessy, A. Mandelis, J. Batista, J. Garcia, J. Appl. Phys. **95**, 7832 (2004)
7. C. Wang, A. Mandelis, J. Tolev, B. Burchard, J. Meijer, J. Appl. Phys. **101**, 123109 (2007)
8. A. Mandelis, J. Batista, D. Shaughnessy, Phys. Rev. B **67**, 205208 (2003)
9. A. Salnick, A. Mandelis, J. Appl. Phys. **80**, 5278 (1996)